Liquid Cooling Technology

Leveraging FloTHERM to design a Compact Liquid Cooling System for High Power Microelectronic Devices

By Gongyue Tang, Yong Han, Boon Long Lau, Xiaowu Zhang, and Daniel Min Woo Rhee, Institute of Microelectronics, Agency for Science, Technology and Research, Singapore

Air cooling can provide a simple, low cost, effective, and reliable cooling solution for microelectronic devices. However, with the increase in heat flux dissipation, current air cooling technology is not sufficient for new high power devices. When the heat flux goes beyond 100 W/cm2, air cooling methods become inadequate for most applications. Therefore liquid cooling technology for microelectronic devices with high power chips is required.

There are two major modes of liquid cooling technology; single-phase cooling and two-phase cooling.

Considering the higher pressure drop and complexity of a two-phase liquid cooling system, utilizing the single-phase liquid cooling technology for high-heat-flux microprocessors is an attractive option. For a single-phase liquid cooling technology, both microchannel and microjet heat sinks can dissipate high heat fluxes found in high-power electronic devices. Compared with the impinging microjets, microchannel cooling has a lower averaged heat transfer coefficient but the coolant in microchannels can exchange energy with a larger effective surface area with multiple walls within each of the channels. Combining these approaches into a hybrid microcooler would be the ideal approach.

The proposed liquid cooling system includes three major components:

1. A silicon-based hybrid microcooler with multiple drainage microtrenches (MDMTs);
2. A customized compact liquid-to liquid heat exchanger; and
3. A commercial micropump.

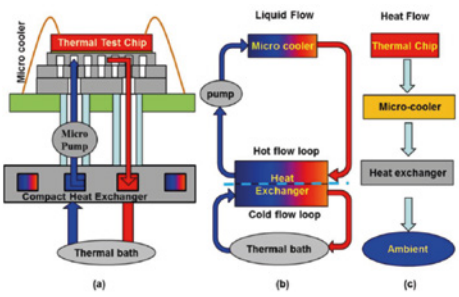

Figure 1. Schematic of the compact liquid cooling system. (a) Concept design of the system. (b) Liquid flow loops in the system. (c) Heat flow path in the system.

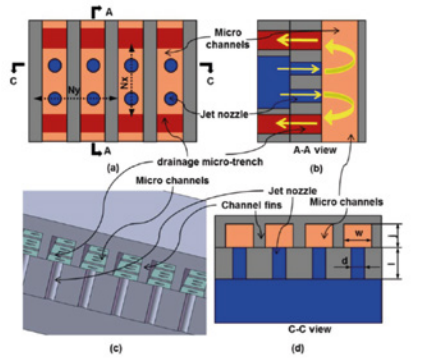

Figure 2. Schematic of the proposed hybrid microcooler with MDMTs design. (a) Pattern of the microchannels, jet nozzles, and MDMTs. (b) Side view of the A—A cross section. (c) 3-D isometric view. (d) C—C cross-sectional view.

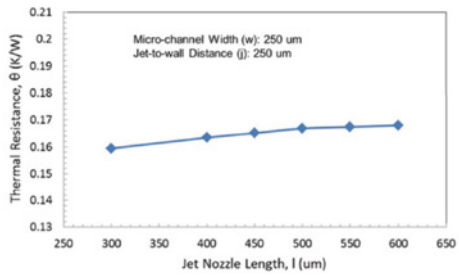

Figure 3. Variation of junction to microcooler thermal resistance with jet nozzle length.

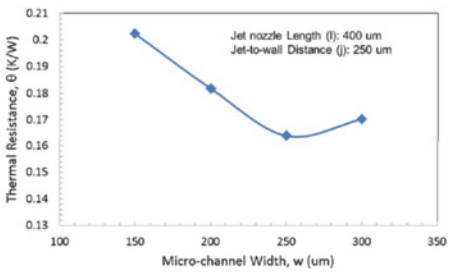

Figure 4. Variation of junction to microcooler thermal resistance with microchannel width.

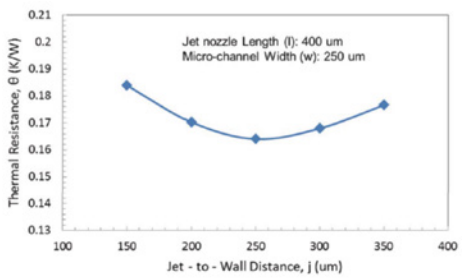

Figure 5. Variation of junction to microcooler thermal resistance with JTW distance.

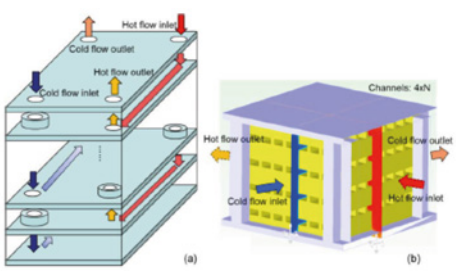

Figure 6. Schematic configurations of the heat exchangers investigated in this paper for (a) counter-flow configuration of commercial heat exchanger A (Hex-A) and (b) cross-flow configuration of customized heat exchanger B (Hex-B).

This article was originally published in Engineering Edge Vol. 5 Iss. 2

A compact liquid cooling system for a microelectronic chip is shown in figure 1(a). It mainly consists of a microcooler to remove the heat from the high performance chip, a commercial micropump to drive the liquid flow, and transport the heat from the chip to an external heat exchanger, where the heat is transferred to the secondary fluid and then rejected to the ambient.

To maximize the performance of the system, the following design criteria should be considered in the design of the proposed liquid cooling system:

1. Avoid large pressure drop the flow rate in the loop at chip cooling side should be maintained at a low level;
2. The heat exchanger should be compact with high heat exchange efficiency, or heat transfer density; and
3. It must maintain the thermal resistance and pressure drop of the heat exchanger at a level obviously lower than that of the microcooler.

A silicon-based microcooler, combining the merits of both microchannels and jet impingement, has been developed to dissipate the heat flux for the high-power IC chip. Figure 2 shows the conceptual design of the hybrid silicon microcooler for the pattern of the microchannels, jet nozzles, and MDMTs. As shown in figure 2(a), there are two nozzles between each of the two trenches in the proposed MDMTs design. The jet flow from the microjet nozzle impinges on the top wall, is constrained to flow along the microchannel, and then exits through the nearby drainage microtrenches.

For this work, the CFD modeling and simulation is conducted using FloTHERM® for the microcooler design optimization. For the chip of size 7 × 7 mm^2, the microjet array is designed to cover an area of 8 × 8 mm^2 for the cooling. The jet nozzle diameter is fixed at 100 µm. The nozzle length, microchannel width, and jet to wall distance are varied in the modeling to evaluate their effects on the thermal performance of the microcooler. Other parameters include nine drainage trenches with a width of 150 µm, 16 nozzles along the microchannel direction and 21 jet nozzles along the drainage trench direction. The coolant in the microcooler is water with an inlet temperature of 25°C. A heat source of 175 W is set for the thermal chip, and a gauge pressure of 20 kPa is set at inlet of the microcooler. A mesh of one million cells is generated, and a grid independence study is conducted. The mesh number is sufficient to obtain accuracy within around 1% for hydraulic and thermal performance. The effects of the nozzle length, microchannel width, and JTW distance on the thermal performance of the microcooler are, respectively, presented in figures 3–5.

A liquid–to-liquid heat exchanger was chosen because it has the advantage of higher heat exchange efficiency, smaller size, and centralized management of the secondary liquid flow through facility cooling, such as a coolant distributed unit.

Two liquid-to-liquid heat exchanger configurations are investigated in the present case. The first heat exchanger (Hex-A) is commercially available with a counter-flow configurations, and it is used as a benchmark to design and optimize the second heat exchanger (Hex-B). Hex-B is a customized compact heat exchanger, which represents the cross-flow configuration, consisting of mini-channel layers alternatively stacked for both the hot and cold fluid flows. Hex-A is with the counter-flow configuration, as shown in figure 6(a); the hot fluid and cold fluid layers are stacked alternatively, separated with metal plates. There are a total of 11 stainless steel (SS) layers, including the top and bottom

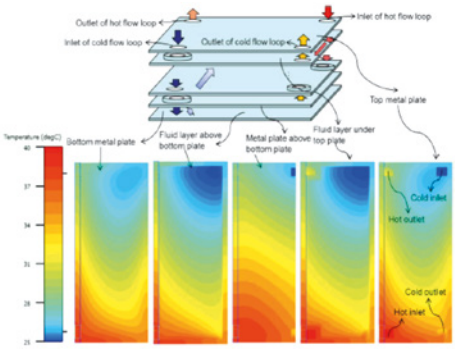

Figure 7. Simulation results of the temperature profiles in the commercial heat exchanger A.

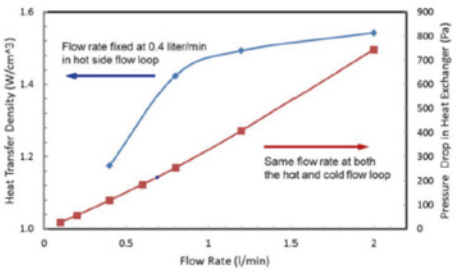

Figure 8. Variation of the heat transfer density, and pressure drop with the rate in Hex-A at the specified conditions.

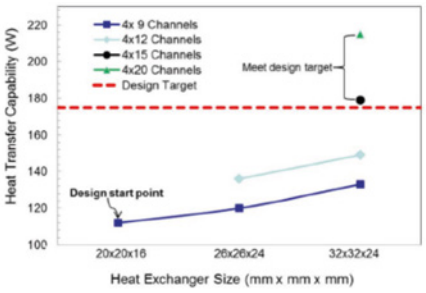

Figure 9. Variation of the heat transfer capability with the channel number's and footprint size of Hex-B at the specified conditions,

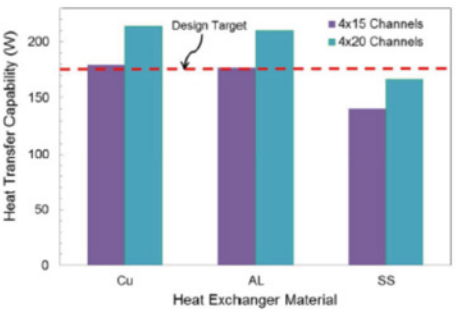

Figure 10. Effect of the material on the heat transfer capability of Hex-B at specified conditions.

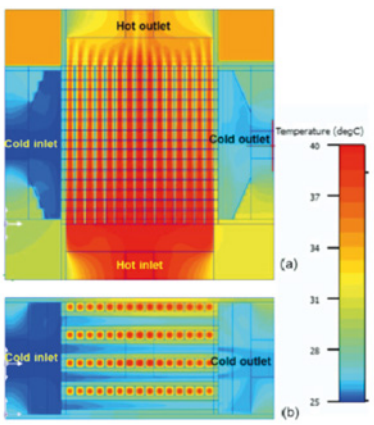

Figure 11. Simulation results of temperature profile for Hex-B with the final design at the specified condition. (a) Top plane view. (b) Side plane view.

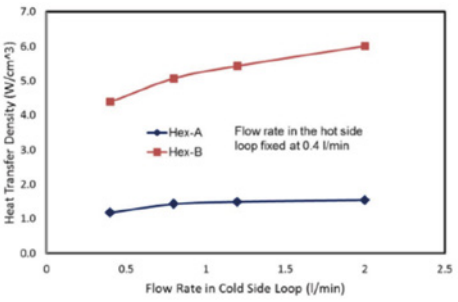

Figure 12. Comparison of heat transfer density for Hex-A and Hex-B at the specified conditions.

This article was originally published in Engineering Edge Vol. 5 Iss. 2

cover plates with a thickness of 1.1 mm for each layer.

These metal layers form ten layers of liquid channels, which include five layers for the cold liquid and five layers for the hot liquid. The overall size of Hex-A is of 204 mm long by 74 mm wide by 25 mm high. Hex-B is designed with cross-flow configuration, as shown in figure 6(b), in which the hot fluid and cold fluids are stacked, with the two types of flow channels arranged at an angle of 90°.u. Hex-B is targeted to have similar performance as Hex-A while have smaller footprint size than that of the Hex-A. FloTHERM is utilized to simulate the thermal and flow profiles in the heat exchangers.

The inlet flow rate is varied from 0.4 to 2 L/ min with a fixed temperature of 25°C for the cold flow loop of the heat exchangers, whereas the flow rate is fixed to 0.4 L/min for the hot flow loop. The inlet flow temperature in the hot flow loop of the heat exchanger is fixed to 40°C for case study.

Due to the relatively small Reynolds number, the laminar flow is assumed. A mesh of 530 K is generated and the grid independence study is conducted. The fields of flow, pressure, and temperature are obtained through the modeling and simulation; as such the liquid temperature at different locations can be captured through the obtained temperature profiles. The performance of Hex-A is used to benchmark the performance of optimized Hex-B. Figure 7 shows the simulation results of the temperature profile in Hex-A. In this case, the flow rate is 0.4 L/min in both the cold flow loop and the hot flow loop; the inlet fluid temperature is of 25°C in cold flow loop and 40°C in the hot flow loop of the heat exchanger.

The heat transfer density is extracted to evaluate the thermal effectiveness of the heat exchangers. The variation of the heat transfer density with liquid flow rate for Hex-A is shown in figure 8. The flow rate in the hot flow loop is fixed at 0.4 L/min. The inlet fluid temperature is 25°C for the cold flow loop and 40°C for the hot flow loop. The heat transfer density is sensitive to flow rate when the flow rate is low (e.g., less than 1 L/min), and less sensitive to the flow rate when the flow rate is high. The pressure drop in the heat exchanger is also important to the cooling system. The variation of the pressure drop with the flow rate for Hex-A is also shown in figure 8. The flow rates in the hot flow loop and cold flow loop remain the same. As expected, the pressure drop in the heat exchanger increases with an increase in the flow rate.

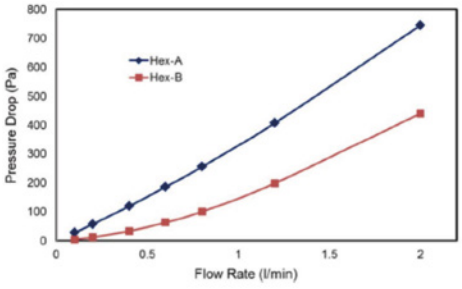

Figure 13. Comparison of pressure drop for Hex-A and Hex -B at the specified conditions.

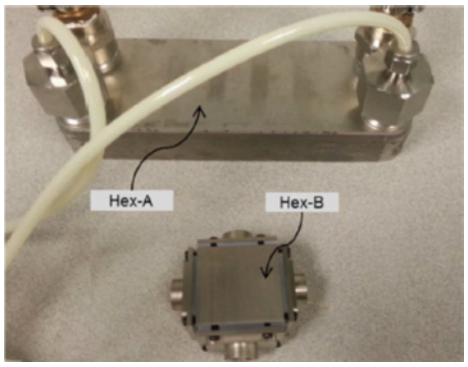

Figure 14. Comparison of the footprint size between the commercial Hex-A and the customized Hex -B

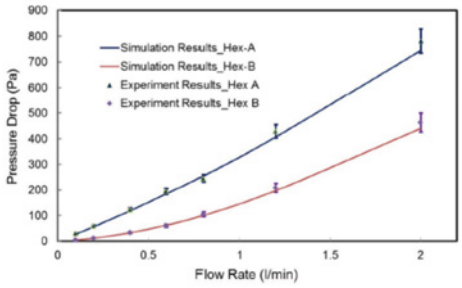

Figure 15. Pressure drop in commercial heat exchanger (Hex-A) and customized compact heat. exchanger (Hex-B).

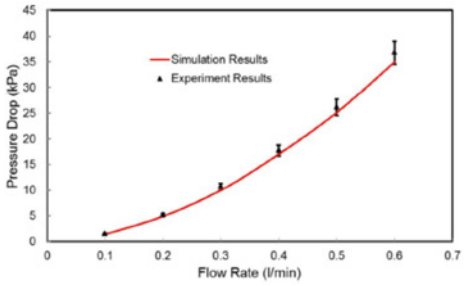

Figure 16. Pressure drop in Microcooler

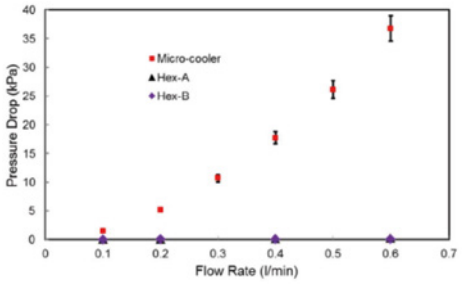

Figure 17. Comparison of the measured pressure drop in microcooler and heat exchangers.

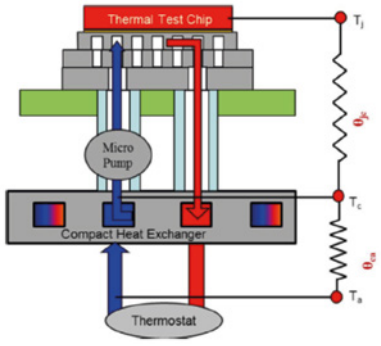

Figure 18. Schematic of the system thermal resistance analysis.

To design the compact Hex-B, the simulation model is first built with 4 × 9 channels in each fluid side with a footprint size of 20 × 20 mm as the design start point. The 6 × 6 cells are assigned in each channel cross section to ensure the computational accuracy, and the grid independent solution is obtained with a mesh number of 1.2 million cells. The simulation results are shown in figure 9. Hex-B with initial configuration, only provides about 110 W heat transfer capability under the specified conditions, which is too low for system design target. Therefore, the design is further optimized to increase the power dissipation capability.

The optimization for Hex-B includes: an increase in channel numbers, an increase in the footprint size and a different the material with higher thermal conductivity. Figure 9 shows the effect of channel numbers and footprint size on thermal performance of the Hex-B. The thermal performance increases as the channel number and footprint size increase. For the heat exchangers with a footprint area of 32 × 32 mm and a channel number of ≥15, their heat transfer capability exceeds the design power of 175W, meeting the design target. The effect of heat exchanger material type is shown in Figure 10. The SS, with a thermal conductivity of 16 W/mK, would have unfavorable thermal performance below the design target, which is not preferred material for Hex-B. Additionally, the aluminum heat exchanger has similar thermal performance as that for the copper heat exchanger. Hence, the aluminum heat exchanger is suggested for practical fabrication due to the light weight.

Based on the above analysis, the optimized heat exchanger has a footprint area of 32 × 32 mm with a channel number of 15 in each row for both fluids, and is made of aluminum. Figure 11 shows the simulation results of the temperature profile for Hex-B with the final design.

To assess the effectiveness of the design of Hex-B, the heat transfer density and the pressure drop of Hex-B are compared with those of Hex-A. Figure 12 presents the comparison of the heat transfer density between Hex-A and Hex-B at the specified conditions. Figure 13 shows the comparison of the pressure drop in Hex-A and Hex-B at the specified conditions.

Compared with the Hex-A, the much higher heat transfer density and the much lower pressure shown for Hex-B, affirm the high effectiveness of this compact heat exchanger. The optimized Hex-B is made of aluminum and includes dual flow channels for both hot fluid and cold fluid. Silicone rubber was used as a sealing ring. The weight of the newly fabricated heat exchanger is 0.23kg with all the connecting flanges, which is much less than that for the Hex-A, which weighs 1.20 kg. Additionally, the footprint area of the newly fabricated heat exchanger is much smaller than that of Hex-A, as shown in figure 14. The optimized compact Hex-B has larger heat transfer area ratio and effectiveness.

Another major objective of the design of the liquid cooling system is to reduce the system pressure drop so as to achieve the compactness of the system by selecting the micropump with low pumping power and small size. The variation of the simulated and measured pressure drops versus the flow rate in the heat exchangers and microcooler are presented in figures 15 and 16, respectively. This shows that the experimentally measured pressure drop agrees reasonably well with the simulated value, and the simulated results are slightly lower (5%~10%) than the measured values. The pressure drop in the newly designed and fabricated compact Hex-B is about half of the pressure drop in the Hex-A. It can also be seen that the microcooler with microjet nozzle and microchannels is the main contributor to the pressure drop of the full system, accounting for around 97~99% of the system pressure drop. The proportions of system pressure drop in the microcooler and heat exchanger are shown in figure 17. This indicates that the hydraulic design of this system is efficient, and the pressure drop in the heat exchanger has been reduced to a reasonable level.

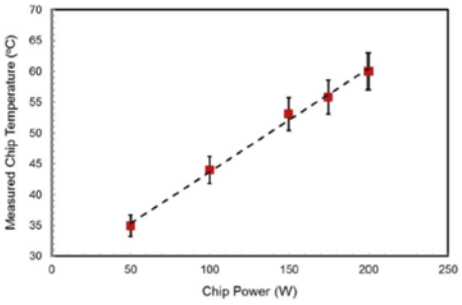

Figure 19. Measured chip temperature through the IR camera for different chip powers.

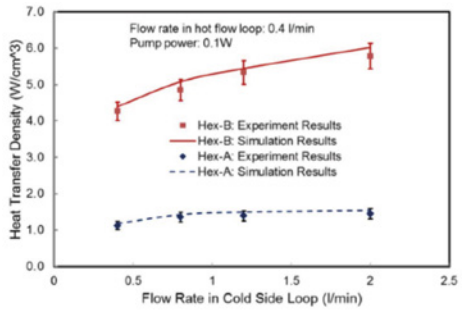

Figure 21. Measured thermal transfer density for commercial heat transfer A and compact Hex -B (a power of 175 W).

The thermal resistance is extracted to evaluate the thermal performance of the full system. The schematic 1-D thermal network of the system is shown in Figure 18. It is seen that the junction to ambient thermal resistance of the system (θ_{ja}) consists of two parts; the first part is the thermal resistance from the junction to microcooler (θ_{jc}), which represents the thermal performance of the microcooler and the other is the thermal resistance from the microcooler to the ambient (θ_{ca}), which represents the thermal performance of the heat exchanger.

The design target for this silicon microcooler system is to have a heat dissipation capability of 350 W/cm^2, which corresponds to a heat power of 175 W on a 7 × 7 mm chip. Assuming the system works in an environment of 40°C, and the allowable junction temperature is 85°C. The design target of the junction to ambient thermal resistance for this system is about 0.25°C/W.

In the tests, the power applied to the thermal test chip varies from 50 to 200 W. The chip temperature under different chip powers is measured, and the results are shown in figure. 19. The flow rate remains 0.4 L/ min in the hot loop and 2 L/min in the cool loop during the test. It can be seen that the chip temperature linearly increases with the increase in the power applied to the chip, while, the overall thermal resistance of the

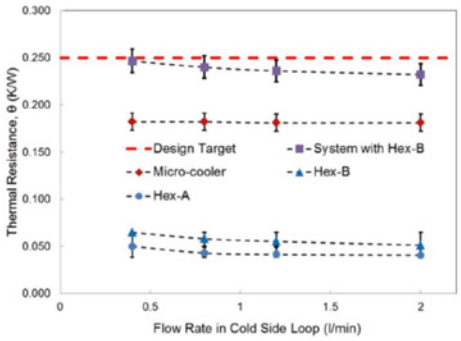

Figure 20. Measured thermal resistance of the heat exchangers, microcooler, and the full system assembled with compact Hex -B (a power of 175 W).

system, including the thermal resistance of the microcooler and the thermal resistance of the heat exchanger, has been obtained. The results are shown in figure 20. The thermal resistance of the heat exchangers decreases when the flow rate in the cool flow loop increases, as such causing the decrease in the overall system thermal resistance with the increase of the flow rate in the cold flow loop. Taking a close examination to figure 20, it shows that the microcooler is the main contributor to the overall system thermal resistance, accounting for around 80~90% of the total thermal resistance, while the heat exchanger only accounts for about 10~20% of the overall system thermal resistance. Additionally, the thermal resistance of Hex-B is slightly larger than that for the Hex-A. While Hex-B is much smaller and lighter than Hex-A. Furthermore, the pressure drop in Hex-B is only half of the pressure drop in Hex-A. Furthermore, as shown in figure 21, the heat transfer density of Hex-B is much higher than that for Hex-A. Hence, it can be concluded that the design of Hex-B is more effective than the design of the Hex-A for the applications in this paper.

Furthermore, the developed compact cooling system is able to meet the design target of 175-W heat dissipation capability with a pumping power of 0.1 W.

Reference:

IEEE TRANSACTIONS ON COMPONENTS, PACKAGING AND MANUFACTURING TECHNOLOGY, VOL. 6, NO. 5, MAY 2016

Development of a Compact and Efficient Liquid

Cooling System With Silicon Microcooler for

High-Power Microelectronic Devices

Gongyue Tang, Yong Han, Boon Long Lau, Xiaowu Zhang, Senior Member, IEEE, and Daniel Min Woo Rhee

Mentor Graphics

Mechanical Analysis

This article originally appeared in Engineering Edge Vol. 5 Iss. 2

Download the latest issue: www.mentor.com/products/mechanical/engineering-edge

ENGINEERING EDGE

Accelerate Innovation with CFD & Thermal Characterization

You might also be interested in...